IL NUOVO CIMENTO Vol. 37 C, N. 6 Novembre-Dicembre 2014
DOI 10.1393/ncc/i2015-11845-2

Colloquia: LaThuile14

QCD studies at ATLAS

M. Wielers on behalf of the ATLAS Collaboration
STFC-RAL - Didcot, UK

ricevuto il 31 Luglio 2014

Summary. — There is significant ongoing efforts in ATLAS to better understand QCD effects. These proceedings contain some examples highlighting recent results. Studies were carried out covering a wide range of QCD phenomena, which include the production of ϕ mesons in minimum bias events, processes involving photons and jets, and the measurement of the W plus charm jet production. In these analyses the data are compared at particle-level with theoretical predictions and Monte Carlo simulations. In general, a good agreement between data and the predictions is found for a wide spectrum of observables. Several of the presented results provide input to the tuning of the parton distribution functions.

PACS 12.38.Qk – Quantum chromodynamics: Experimental tests.
PACS 13.85.Rm – Inclusive production with identified photons.
PACS 13.87.-a – Jets in large-Q^2 scattering.

1. – Introduction

The high cross sections for Standard Model (SM) processes produced in proton-proton (pp) collisions at the Large Hadron Collider (LHC) allow one to measure precisely the effects of perturbative quantum chronodynamics (QCD), to test the predictions of various Monte Carlo (MC) generators and understood better low-energy non-perturbative effects. Many of these measurements can help to constrain the gluon or quark parton distribution functions (PDF) of the proton. Other studies allow one to measure the strong coupling constant (α_s) or to test the dynamics of the hard scattering process.

The results presented in these proceedings are based on proton-proton collisions collected with the ATLAS detector [1] at a centre of mass energy $\sqrt{s} = 7\,\text{TeV}$ using an integrated luminosity of around $36\,\text{pb}^{-1}$ and $4.6\,\text{fb}^{-1}$, respectively. The measured cross sections are corrected for detector effects to the particle-level in a fiducial volume chosen as close as possible to the detector acceptance. These distributions are compared to the predictions of MC generators, which include models for parton hadronisation as well as multiple parton interactions and parton-level predictions corrected for non-perturbative effects at particle-level.

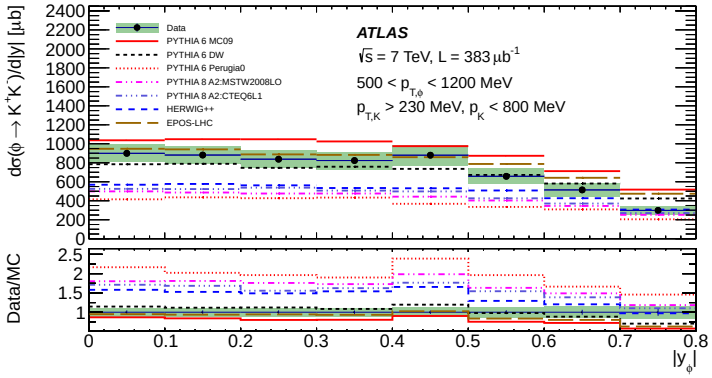

Fig. 1. – Fiducial cross section of the $\phi(1020)$-meson as a function of $|y^{\phi}|$. The error bars represent the statistical uncertainty and the green boxes represent the quadratic sum of the statistical and systematic uncertainties. The 3.5% uncertainty on the luminosity is not included. The data are compared to various MC expectations as described in the legends. From [2].

In the following, examples are shown from the different areas of QCD studies. Section **2** reports on the cross section measurements of the $\phi(1020)$ meson in soft interactions. Section **3** shows results from the measurement of the dijet and multijet cross section. Like the measurement of the dijet cross section the direct prompt photon production process (presented in sect. **4**) can also shed light on the gluon PDFs. The production of a W boson in association with a charm quark constrains the strange-quark PDF and tests the strange-quark asymmetry of the quark sea and is summarised in sect. **5**.

2. – Cross section measurement of the $\phi(1020)$ meson in soft interactions

The differential production cross section of the $\phi(1020)$-meson was measured using $383\,\mu\text{b}^{-1}$ of minimum-bias events collected in 2010 [2]. This measurement provides input to the tuning and development of phenomenological models. ϕ-mesons are produced from strange sea quarks, from gluon fusion and from the fragmentation process, the latter being a non-perturbative process. In this study ϕ-mesons from the decay mode $\phi \to K^+K^-$ mesons are reconstructed. The kaons are identified by their energy loss in the pixel detector. The differential cross section is measured as a function of the transverse momentum, p_T^{ϕ}, and rapidity, y^{ϕ} of the ϕ-meson in the fiducial range $500 < p_T^{\phi} < 1200\,\text{MeV}$, $|y^{\phi}| < 0.8$, $p_T^K > 230\,\text{MeV}$ and $p^K < 800\,\text{MeV}$. The integrated cross section in this fiducial range is $\sigma_{\phi\to K^+K^-} = 570 \pm 8(\text{stat}) \pm 66(\text{syst}) \pm 20(\text{lumi})\ \mu\text{b}$. As an example, fig. 1 shows the cross section as a function of p_T^{ϕ} together with the predictions from the MC generators Pythia-6, Pythia-8, Herwig++ and EPOS and using different generator tunes. As can be seen there is some discriminating power between the different models, with the cross section being best described by the Pythia-6 tune DW and by the EPOS-LHC tune. Pythia-6 predictions using different tunes differ significantly and the cross section is underestimated by both PYTHIA-8 and Herwig++.

3. – Measurement of the dijet and multijet cross section

Using the $4.5\,\text{fb}^{-1}$ of data collected in 2011, the double-differential dijet cross section was measured as functions of the dijet mass m_{12} and rapidity separation of the two

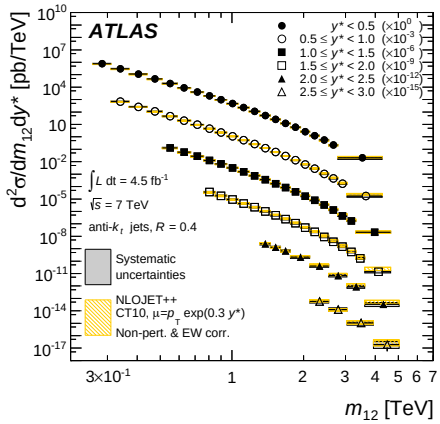

Fig. 2. – Dijet double-differential cross sections for anti-k_T jets with a cone size $R = 0.4$ as a function of dijet mass in different ranges of y^*. To aid visibility, the cross sections are multiplied by the factors indicated in the legend. The error bars indicate the statistical uncertainty, and the dark-shaded band the experimental systematic uncertainties. For comparison, the NLO QCD predictions of NLOJet++ are included. The hatched band shows the uncertainty associated with the theory predictions. Because of the logarithmic scale on the vertical axis, the uncertainties are only visible at high dijet mass, where they are largest. From [3].

highest-p_T jets ($y^* = |y_1 - y_2|/2$) [3]. In the analysis, the anti-k_T algorithm with cone sizes of $\Delta R = \sqrt{(\Delta\eta)^2 + (\Delta\phi)^2} = 0.4$ and 0.6 was used. Figure 2 shows this cross section, which is measured up to dijet masses of 5 TeV and y^* of 3.0, using jets with $\Delta R = 0.4$. The cross section, which decreases quickly with increasing dijet mass, are compared to next-to-leading order (NLO) QCD calculations with NLOJet++ using the CT10 PDF set and corrected for non-perturbative and electroweak effects. No major deviation of the data from these predictions is observed over the full kinematic range, covering almost eight orders of magnitude in measured cross-section values. The measurements in the high-mass region can be used in the future to constrain the PDFs at high momentum fractions. The results are also compared with the predictions from NLOJet++ using the PDF sets CT10, HERAPDF1.5, epATLJet13, MSTW 2008, NNPDF2.1, NNPDF2.3, and ABM11. Some of these comparisons are shown in fig. 3. A good agreement is seen for most PDF sets. Disagreement is observed at high dijet mass in some ranges of y^* when using the HERAPDF1.5 PDF set, and an even stronger disagreement is found using ABM11.

Another interesting process is the multijet production as it probes the dependence of the theory prediction on higher-order terms. In this analysis [4], which uses 35 pb^{-1} of data taken in 2010, events with two or three jets are selected using the anti-k_T algorithm with $\Delta R = 0.6$. The jets must have $p_T > 40$ GeV and lie in $|y| < 2.8$ with $p_T > 60$ GeV for the leading jet. The ratio $R_{3/2}(p_T^{\rm lead})$ is measured. $R_{3/2}(p_T^{\rm lead})$ is defined as $R_{3/2}(p_T^{\rm lead}) = (\mathrm{d}\sigma_{N_{\rm jet}\ge 3}/\mathrm{d}p_T^{\rm lead})/(\mathrm{d}\sigma_{N_{\rm jet}\ge 2}/\mathrm{d}p_T^{\rm lead})$, which is the cross section for events with at least three jets over the cross section with at least two jets as a function of the jet-p_T. The results are shown in fig. 4 together with NLO perturbative QCD (pQCD) predictions, corrected for non-perturbative effects and obtained with $\alpha_s(M_Z) = 0.110$ and 0.130. The predictions describe well the data, except for $p_T^{\rm lead} < 140$ GeV.

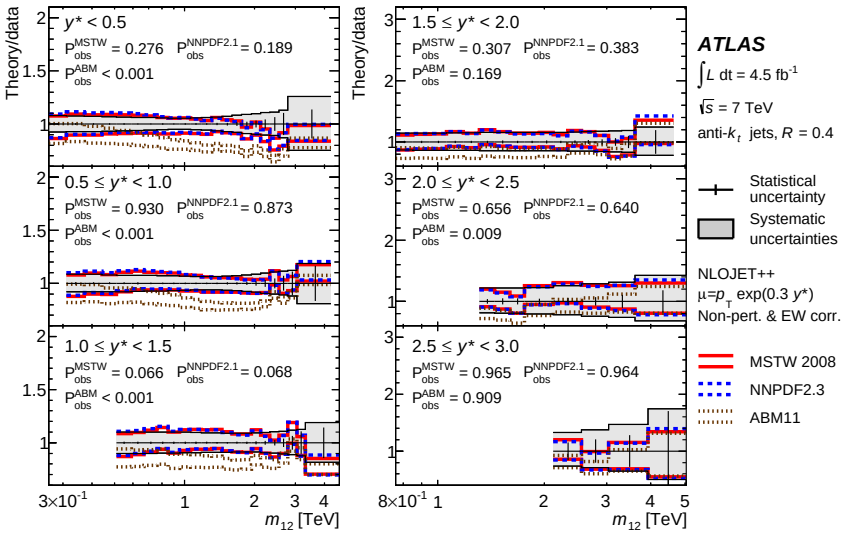

Fig. 3. – Ratio of the NLO QCD predictions of NLOJet++ to the measurements of the dijet double-differential cross section as a function of dijet mass in different ranges of y^*. The results are shown for jets identified using the anti-k_T algorithm with radius parameter $R = 0.4$. The predictions of NLOJet++ using different PDF sets are shown. The renormalisation and factorisation scale choice is $\mu = \mu_R = \mu_F = p_T^{max} e^{0.3y^*}$. Observed probabilities resulting from the comparison of theory with data are shown considering all mass bins in each range of y^* separately. From [3].

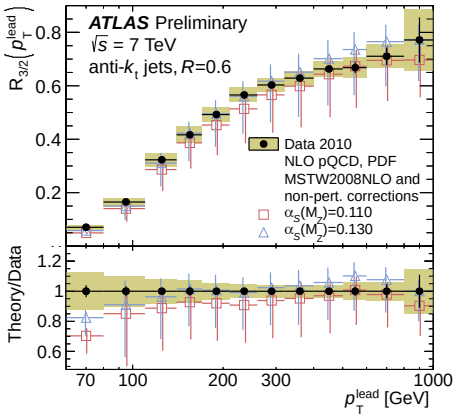

Fig. 4. – Measurement of $R_{3/2}$ as a function of $p_T^{\rm lead}$. NLO pQCD theoretical predictions, corrected for non-perturbative effects, are shown for $\alpha_s(M_Z) = 0.110$ and 0.130. The black error bars correspond to the statistical uncertainty on the measured values while the yellow bands correspond to the total experimental uncertainty. The red and blue error bars correspond to the total theoretical uncertainty on the respective NLO perturbative QCD theoretical predictions, obtained by summing in quadrature the uncertainty from the non-pQCD correction, PDFs and scales. They are offset horizontally for clarity. From [4].

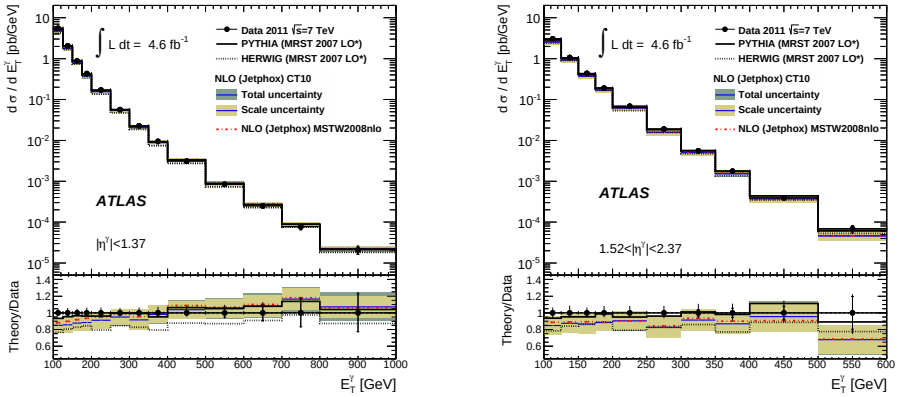

Fig. 5. – Measured (dots with error bars) and expected inclusive prompt photon cross section as a function of the photon transverse energy in $|\eta^\gamma| < 1.37$ (left) and $1.52 < |\eta^\gamma| < 2.37$ (right). The inner error bars on the data points show statistical uncertainties, while the full error bars show statistical and systematic uncertainties added in quadrature. The NLO theory prediction is shown with the shaded bands indicating the scale uncertainty (inner yellow band) and the total uncertainty (outer green band), the latter also includes the PDF and α_s uncertainties. The MC generators are shown as lines. The bottom panel shows the corresponding theory/data ratio, in which the data points are centered at one. From [7].

$N_{3/2}$ is defined as $N_{3/2}(p_T^{\text{jet}}) = \sum_i^{N_{\text{jet}}}(\mathrm{d}\sigma_{N_{\text{jet}}\geq 3}/\mathrm{d}p_{T,i}) / \sum_i^{N_{\text{jet}}}(\mathrm{d}\sigma_{N_{\text{jet}}\geq 2}/\mathrm{d}p_{T,i})$, where i is the bin number. This ratio is obtained by dividing the jet-p_T distribution for events with at least three jets, by that of events with at least two jets. Note, $N_{3/2}$ receives one entry per jet. Like $R_{3/2}$, this quantity is proportional to the strength of α_s but is less sensitive to the choice of the renormalisation and factorisation scale. Using the measurements in $210\,\text{GeV} < p_T^{\text{jet}} < 800\,\text{GeV}$, a least-squares fit is performed both individually in each p_T^{jet} bin and by simultaneously fitting all of them. The combined fit results in a value of $\alpha_s(M_Z) = 0.111 \pm 0.006(\text{exp})^{+0.016}_{-0.003}(\text{theory})$. This value is in good agreement with the $\alpha_s(M_Z)$ world average value of 0.1184 ± 0.0007 [5, 6]. The measured energy scale dependence of α_s up to a scale of 800 GeV is also compatible with the evolution predicted by the Renormalisation Group Equation.

4. – Measurement of the prompt photon cross section

The inclusive prompt photon cross section, which arises from photons from the direct production and from photons from fragementation, was measured in ATLAS using $4.5\,\text{pb}^{-1}$ of data taken in 2011 [7]. The photons must be isolated and fulfill $E_T < 7\,\text{GeV}$ in a cone of radius 0.4 in $\eta - \phi$ space around the photon. Figure 5 shows the cross section as a function of the transverse energy E_T^γ in the kinematic range $100 < E_T^\gamma < 1000\,\text{GeV}$ and $|\eta^\gamma| < 1.37$ and $1.52 < |\eta^\gamma| < 2.37$. The predictions of the leading order (LO) parton-shower MC generators, Pythia and Herwig, are also shown. As can be seen, the Pythia model describes the data fairly well, while Herwig is 10%–20% below the data. The shapes of the cross sections are well described by both models. The NLO calculations agree with the data within the theoretical uncertainty. However, there is the tendancy for the data points to be somewhat higher than the central NLO calculation at low E_T^γ.

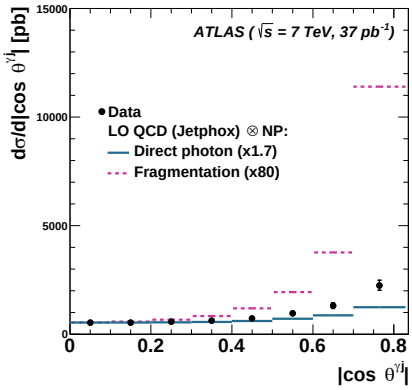

Fig. 6. – The bin-averaged cross section for isolated-photon plus jet production (dots) as a function of $|\cos\theta^{\gamma j}|$. The direct-photon (solid lines) and fragmentation (dashed lines) components of the LO QCD prediction are also included. The calculations were normalised to the measured cross section for $|\cos\theta^{\gamma j}| < 0.1$; the factors used are shown in parentheses. From [9].

These measurements can potentially constrain the shape and uncertainty of the gluon PDF in $0.03 < x < 0.3$ [8] due to the large theoretical PDF uncertainties at high E_T^γ.

Another good test of pQCD effects is the study of the isolated-photon plus jet cross sections. This has been measured as functions of photon transverse energy, jet transverse momentum and jet rapidity using $37\,\text{fb}^{-1}$ of data taken in 2010 [9]. Events were selected containing photons with $E_T^\gamma > 45\,\text{GeV}$ in $|\eta^\gamma| < 2.37$ excluding $1.37 < |\eta^\gamma| < 1.52$. The photon is combined with the leading jet for jets with $p_T > 40\,\text{GeV}$. Good agreement is observed compared with the Jetphox predictions, using multiple PDF sets. In addition, the cross section as a function of the difference between the azimuthal angles $|\cos\theta^{\gamma j}|$ of the photon and the jet is measured. This angle corresponds to the angle in the $2 \to 2$ hard-scattering process and is sensitive to a quark or gluon exchange. As can be seen in fig. 6, the shape of the measured cross section $\mathrm{d}\sigma/\mathrm{d}|\cos\theta^{\gamma j}|$ is much closer to that of the direct photon process than that of the fragmentation. This is consistent with the dominance of a quark exchange.

5. – Production of W bosons in association with charm quarks

The cross section of a W boson together with a single charm quark is measured using $4.6\,\text{fb}^{-1}$ of data [10]. The W boson is identified via its decay to an electron or muon and neutrino. The charm quark is tagged via a low-p_T muon from a semileptonic decay inside a jet or by the presence of a $D^{(*)}$ meson. The charge correlation between the lepton from the W and the $D^{(*)}$ is used to extract the single-charm component. The cross section is calculated by subtracting the same charge (SS) distributions from the opposite charge (OS) one. The yield is found by fitting the $D^\pm$ mass (for $D^\pm$) or the $D^* - D^0$ mass difference (for $(D^{*\pm}$). The cross sections are measured in the region $p_T^l > 20\,\text{GeV}$, $|\eta^l| < 2.5$, $p_T^\nu > 25\,\text{GeV}$, $m_T^W > 40\,\text{GeV}$. In addition, for $W + c$-jet events the jets need to fulfill $p_T^j > 25\,\text{GeV}$ and $|\eta^j| < 2.5$ while for the $W + D^{(*)}$ channel $p_T^{D^{(*)}} > 8\,\text{GeV}$ and $|\eta^{D^{(*)}}| < 2.2$. The cross section for $W + c$-jet and $W^\pm + D^{(*)\mp}$ events are shown in fig. 7. The plots also show a comparison with predictions from aMC@NLO using different PDF

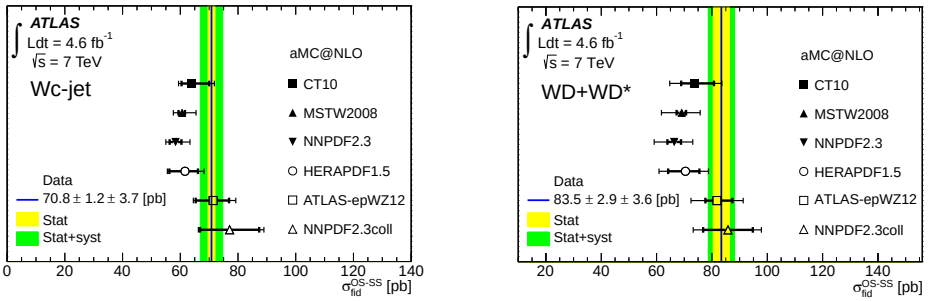

Fig. 7. – Measured fiducial cross sections $\sigma^{OS-SS}(W + D^{(*)})$ (right) and $\sigma^{OS-SS}(W + c\text{-jet})$ (right) compared to different PDF predictions based on aMC@NLO. The solid vertical line shows the central value of the measurement, the inner error band corresponds to the statistical uncertainty and the outer error band to the sum in quadrature of the statistical and systematic uncertainties. The PDF predictions are shown by markers. The inner error bars on the theoretical predictions show the 68% confidence level uncertainties obtained from the error sets provided with each PDF set, while the outer error bar represents the total theoretical uncertainty (sum in quadrature of PDF, parton shower, fragmentation and scale uncertainties). From [10].

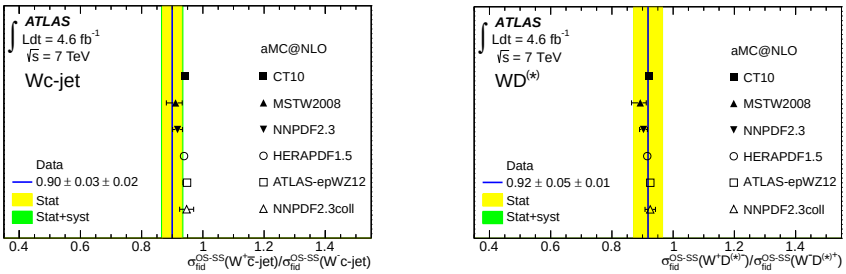

Fig. 8. – $R_c^{\pm}$ measurement in the $W + c$-jet (left) and $W + D^{(*)}$ (right) channel compared to various PDF predictions based on aMC@NLO. The blue vertical lines show the central values of the measurements, the inner error bands show the statistical uncertainties and the outer error bands the total experimental uncertainties. The PDF predictions are shown by the black markers. The error bars on the predictions correspond to the 68% CL PDF uncertainties.

sets. CT10, MSTW2008, NNPDF2.3, HERAPDF1.5 use a suppressed strangeness([1]) contribution. epWZ, which include the ATLAS W and Z boson measurements, has a strangeness contribution equal to u and d-sea quarks. NNPDF2.3coll, which includes only collider data, has an even more enhanced strange-quark contribution than epWZ. The measurement is most consistent with predictions using epWZ and NNPDF2.3coll, both of which have enhanced strangeness as compared to the other PDF sets.

The cross section ratio $R_c^{\pm} = \sigma^{OS-SS}(W^+\bar{c})/\sigma^{OS-SS}(W^-c)$ is sensitive to a possible strange-antistrange quark asymmetry. A deviation from unity is caused by two effects. As the proton contains valence d-quarks, the Cabbibo suppressed diagrams involving

([1]) Although in CT10 the strange contribution is less suppressed than in the others.

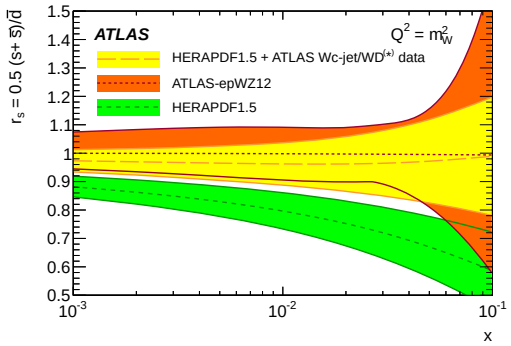

Fig. 9. – Ratio of strange-to-down sea-quark distributions r_s as a function of x as assumed in HERAPDF1.5 PDF compared to the ratio obtained from the fit including the ATLAS $W + c$-jet/$W + D^{(*)}$ data and the ratio obtained from ATLAS-epWZ12. The error band on this measurement represents the total uncertainty. The ratio r_s is shown at $Q^2 = m_{W^2}$. From [10].

d-quarks enhance $W^+ + c$-jet production over $W^- + c$, thereby decreasing $R_c^{\pm}$. Secondly, a difference between s and $\bar{s}$ PDFs, as suggested by neutrino data [11], influences the value of the ratio and can push it to a lower value. This effect is implemented in both NNPDF2.3 and MSTW2008, with a larger contribution for MSTW2008. This pattern of predictions is consistent with those obtained from the NLO calculation as implemented in aMC@NLO and shown in fig. 8. CT10 uses symmetric s and $\bar{s}$ distributions. Using the down-to-strange density from this PDF and assuming that the measured deviation from unity of $R_c^{\pm}$ is mainly due to the down quark, one can attribute the total difference $R_c^{\pm}(\text{CT10}) - R_c^{\pm}(\text{Data})$ to the effect of a strange asymmetry. This asymmetry $A_{s\bar{s}}$ is measured to be $(2 \pm 3)\%$ for the combination of the $W + c$-jet and $W + D^{(*)}$ analyses.

The cross section measurements can be also used to measure the strange-to-down sea content of the proton $r_s = 0.5 \cdot (s + \bar{s})/\bar{d}$. This is done using HERAPDF1.5 in which the strange quark distribution is expressed as an x-independent fraction via $f_s = \bar{s}/(\bar{d} + \bar{s})$. This fraction f_s was varied implicitly in HERAPDF1.5 by increasing the uncertainty of the strange fraction f_s. This corresponds to a free fit of f_s while all other parameters are constrained to the default values. The result is shown in fig. 9. The measured distribution of r_s determined in this study is in very good agreement with the results from epWZ and supports the hypothesis of an $SU(3)$ symmetric light quark sea.

REFERENCES

[1] ATLAS Collaboration, *JINST*, **3** (2008) S08003.
[2] ATLAS Collaboration, *Eur. Phys. J. C*, **74** (2014) 2895.
[3] ATLAS Collaboration, *JHEP*, **05** (2014) 059.
[4] ATLAS Collaboration, Tech. Rep. ATLAS-CONF-2013-041 (2013).
[5] Bethke S., *Eur. Phys. J. C*, **64** (2009) 689.
[6] Beringer J. *et al.*, *Phys. Rev. D*, **86** (2012) 010001.
[7] ATLAS Collaboration, *Phys. Rev. D*, **89** (2014) 052004.
[8] ATLAS Collaboration, Tech. Rep. ATLAS-PHYS-PUB-2013-018 (2013).
[9] ATLAS Collaboration, *Nucl. Phys. B*, **875** (2013) 483.
[10] ATLAS Collaboration, *JHEP*, **05** (2014) 068.
[11] NuTev Collaboration, *Phys. Rev. D*, **64** (2001) 112006.